Electron spectroscopy with a commercial 4H-SiC photodiode

Article (Accepted Version)

Accepted Manuscript

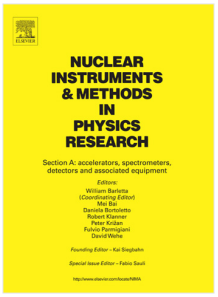

Electron spectroscopy with a commercial 4H-SiC photodiode

S. Zhao, G. Lioliou, S. Butera, M.D.C. Whitaker, A.M. Barnett

PII: S0168-9002(18)31143-4
DOI: https://doi.org/10.1016/j.nima.2018.09.017
Reference: NIMA 61182

To appear in: *Nuclear Inst. and Methods in Physics Research, A*

Received date : 1 June 2018; Revised date : 3 September 2018;
Accepted date : 6 September 2018

Please cite this article as: S. Zhao, et al., Electron spectroscopy with a commercial 4H-SiC photodiode, *Nuclear Inst. and Methods in Physics Research, A* (2018), https://doi.org/10.1016/j.nima.2018.09.017

Electron spectroscopy with a commercial 4H-SiC photodiode

S. Zhao, [1, *], G. Lioliou[1], S. Butera[1], M.D.C. Whitaker[1], A.M. Barnett[1]
[1] Space Research Group, School of Engineering and Informatics, University of Sussex, Brighton BN1 9QT, UK.
[*] Corresponding author, E-mail: Shifan.Zhao@sussex.ac.uk

Keywords: Photodiode; Silicon carbide; COTS; Commercial off the shelf; electron spectroscopy

Abstract
A Commercial-Off-The-Shelf (COTS) 4H-SiC p-n photodiode (sold as a UV detector) was investigated as detector of electrons (β^- particles) over the temperature range 100 °C to 20 °C. The photodiode had an active area of 0.06 mm^2. The currents of the photodiode were measured in dark condition and under the illumination of a ^{63}Ni radioisotope β^- particle source (endpoint energy = 66 keV). The photodiode was then coupled to a custom-made low-noise charge-sensitive preamplifier to make a direct detection particle counting electron spectrometer. ^{63}Ni β^- particle spectra were accumulated with the spectrometer operating at temperatures up to 100 °C. The quantum efficiency of the photodiode as well as the spectrum expected to be detected were calculated via Monte Carlo simulations produced using the CASINO computer program. Comparisons between the simulated and detected ^{63}Ni β^- particle spectra are presented. The work was motivated by efforts to apply COTS technologies to develop low-cost space science instrumentation; a low-cost electron spectrometer of this type could be included on a university-led CubeSat mission for space plasma physics and magnetosphere experiments.

1. Introduction

Many wide bandgap semiconductor materials have been studied for their potential utility as radiation detectors for operation in harsh terrestrial environments and for future space missions. Compared with narrower bandgap semiconductors, e.g. Si (Eg = 1.12 eV at room temperature [1]), the wide bandgap semiconductor silicon carbide (4H-SiC, Eg = 3.27 eV at room temperature [2]) has a higher breakdown field, lower intrinsic carrier concentration, and better carrier saturation velocity [1] [3], which can bring benefits for high temperature operation. Moreover, SiC detectors have high radiation tolerance [4-5], which can be an important feature for both terrestrial and space applications. Therefore, SiC is expected to play a major role in future spacecraft electronics, particularly as a material for semiconductor radiation detectors used in spectrometers.

SiC was first reported as a particle detector in 1999; detectors made from a 310 μm thick semi-insulating 4H-SiC substrate and with different sizes of circular Ohmic contacts (1 mm to 3 mm diameter) were illuminated with a ^{90}Sr β^- particle source [6]. Since then, SiC has been studied intensively for particle detection. SiC particle detectors can have high charge collection efficiencies [7-8], good linear energy response, and excellent energy resolution [9-10]. SiC particle detectors have also shown stability for extended periods and suitability for operation over a wide range of temperatures (27 °C to 227 °C) [11]. Outside of particle detection, significant work developing SiC for photon counting X-ray spectroscopy has been conducted and reported with superb results [12-13]. Recently, SiC p-n photodiodes intended for UV detection have become widely commercially available. With well-developed fabrication technology and high-quality material, low-cost Commercial-Off-The-Shelf (COTS) SiC detectors open the possibility of using SiC detectors for applications such as industrial monitoring (e.g. monitoring and controlling the thickness of materials, and monitoring of spent nuclear fuel assemblies) as well as low-cost space science (e.g. as electron spectrometers to measure the energy and particle density of electrons in low earth orbit and elsewhere). Much valuable work has also been reported considering SiC detectors for use in laser-plasma diagnostics and the related fields [14-17].

Whilst larger space missions (those comparable to ESA Cosmic Vision S-, M-, and L- Class missions) are likely to continue use custom-detectors for the foreseeable future, mass-produced COTS SiC detectors, like those reported here, may be of value to groups developing CubeSat space science missions at universities and other organisations. Previously, results demonstrating the use of commercial 4H-SiC p-n photodiodes for X-ray spectrometers have been reported [18-20]. In this paper, we present work investigating such photodiodes for their suitability as detectors in electron spectrometer at temperatures up to 100 °C.

2. 4H-SiC photodiodes

The 4H-SiC UV p-n photodiode (active area of 0.06 mm^2) was manufactured by sglux SolGel Technologies GmbH, Berlin, Germany [21] and purchased from a standard electronics retailer in the UK. The 4H-SiC structure had an epitaxial layer consisting of a 0.15 μm thick p type layer and a ~5 μm thick n-type layer on top of a 4H-SiC substrate. The geometry of the devices can be found in Ref. [22]. The device was packaged in TO-18 can with UV-transparent window. The window was removed as per Ref. [18] so that the device could be

directly illuminated with the ^{63}Ni radioisotope β^- particle source. Despite the manufacture's stated epilayer thickness (5.15 µm), previous capacitance measurements suggested that the thickness of the device's depletion region was 2.37 µm assuming a parallel place capacitance [19]. However, the X-ray photocurrent measurements in Ref. [19] suggested that the thickness of the detector's active region extended beyond the epilayer to include a portion of the substrate, yielding an apparent active layer thickness of 34.5 µm. However, the leakage current of the detector during the X-ray illuminated measurements may have been greater than that measured before illumination. If this was the case, the photocurrent may have been smaller than the measurement indicated, and thus the thickness of the active region of the detector may have been smaller than the photocurrent measurement implied [19]. Therefore, some doubt existed at the start of the measurements reported in the present manuscript as to whether the active region of the detector was 5.15 µm, 2.37 µm, or 34.5 µm. In this present article, by illuminating the detector with β^- particles we show that the active region of the detector is 5.15 µm; i.e. equal to the manufacturer stated epilayer thickness.

3. Experiments

3.1. Measurements of the detector's leakage current as functions of applied reverse bias

The leakage current of the detector was measured as a function of applied reverse bias from 0 V to 100 V in 1 V increments, at temperatures from 100 °C to 20 °C in steps of 20 °C. To do this, the detector was installed inside a light-tight electromagnetically-shielded box inside a TAS Micro MT Environmental Test Chamber. A dry nitrogen environment (relative humidity < 5%) was maintained inside the chamber in order to eliminate any humidity related effects. A Keithley 6487 Picoammeter/Voltage Source was used to bias the detector. National Instruments Labview software was used to automate the measurements. To ensure thermal equilibrium, the detector was allowed 30 min to stabilise at each temperature before measurements were started. The results are presented in Fig. 1. The leakage current of the detector at 100 V reverse bias and the highest investigated temperature (100 °C) was found to be 44.9 pA ± 0.5 pA (corresponding to leakage current density of 74.9 nA/cm^2 ± 0.9 nA/cm^2). The leakage currents of the device were < 1 pA at temperatures ≤ 40 °C. It should be emphasised that the measured currents include the leakage current of the TO-18 can. The Keithley 6487 Picoammeter/Voltage Source had a measurement uncertainty of ± 0.4 pA; as such, the measurements at 40 °C and 20 °C shown in Fig. 1 are considered to be below the noise floor of the picoammeter.

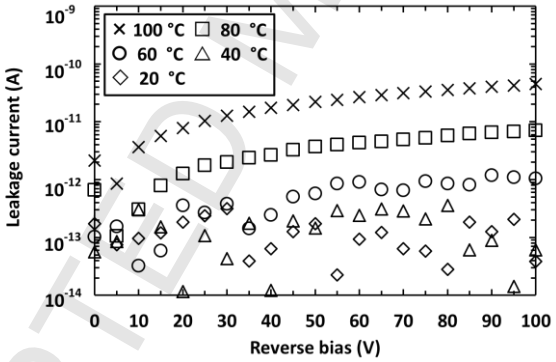

Fig. 1. Leakage currents as functions of applied reverse bias for the 0.06 mm^2 photodiode in the range of temperature from 100 °C to 20 °C.

3.2. Current mode β^- particle measurements

A ^{63}Ni radioisotope β^- particle source (consisting of a 3 µm thick ^{63}Ni layer electroplated onto an ~50 µm thick inactive Ni foil substrate and then covered with a protective 1 µm thick inactive electroplated Ni overlayer) was placed 4.5 mm ± 1.0 mm above the photodiode to investigate the β^- particle response of the photodiode. The ^{63}Ni radioisotope β^- particle source had an active face area of 49 mm^2 and an apparent activity of 136 MBq. The resultant current was measured using the same method as was used for the leakage current measurements (see Section 3.1). The apparent measured β^- particle created current (i.e. the current measured with each device illuminated with the ^{63}Ni radioisotope β^- particle source with the previously measured leakage current subtracted) as a function of applied reverse bias for the device at temperatures from 100 °C to 20 °C is presented in Fig. 2.

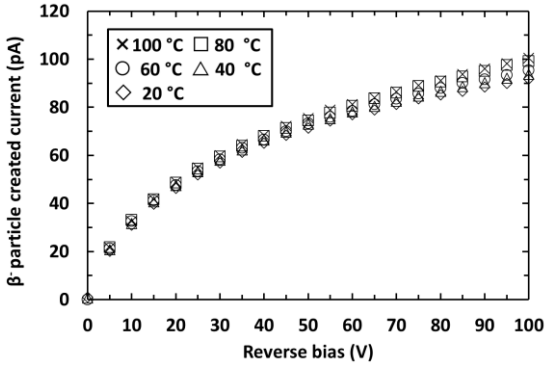

Fig. 2. Measured apparent β^- particle created currents as functions of reverse bias for the 0.06 mm^2 photodiode in the range of temperature from 100 °C to 20 °C.

Previous X-ray measurements with the photodiode suggested that despite the detector having a stated epilayer thickness of 5.15 µm and a depletion region thickness of 2.37 µm (assuming a parallel plate capacitance) [19], collection of charge carriers created by X-rays absorbed substrate may have contributed significantly to the detected signal [19]. These previous measurements suggested that the detector appeared to have an active region which was 34.5 µm thick [19]. Therefore, to compare with the experimental results, calculations were performed to predict the β^- particle created current expected to be detected under the circumstances that the active region thickness was (a) 5.15 µm, (b) 2.37 µm, and (c) 34.5 µm. The expected β^- particle created current, *I*, was calculated using,

$$I = \sum_{i=1(keV)}^{end\ point=66(keV)} \frac{A}{2} E_{mi} \frac{A_{SiC}}{A_{Ni}} DE_i \frac{i}{\omega_{SiC}} q \qquad \text{Eq. 1}$$

which included consideration of the apparent activity of the ^{63}Ni radioisotope β^- particle source (136 MBq), i.e. including the self-absorption, *A* (in units of Bq) [23], the emission probability of the ^{63}Ni radioisotope β^- particle source adjusted for self-absorption, E_{mi} (a dimensionless quantity) [24], the ratio of the area of the detector (0.06 mm^2) and the source (49 mm^2 ± 0.2 mm^2), A_{SiC}/A_{Ni} , the percentage of each electron energy deposited in the active region of the detector, considering the losses in the inactive 1 µm Ni overlayer of the source and the 4.5 mm ± 1.0 mm dry N_2 atmosphere between the source and the detector, and the quantum efficiency of the detector, DE_i (a dimensionless quantity). The quantum efficiency simulations on which the calculations were based are described in Section 4. The electron-hole pair creation energy, ω_{SiC} (in units of eV), was assumed to be 7.8 eV [3] at room temperature. The elementary charge, q, was taken as 1.6×10^{-19} C.

The predicted β^- particle created current of the 0.06 mm^2 photodiode at room temperature was calculated to be 12.5 pA assuming a 5.15 µm thick active region, 9.2 pA assuming a 2.37 µm active region, and 13.8 pA assuming a 34.5 µm thick active region. However, the experimentally measured β^- particle created current of the 0.06 mm^2 photodiode was found to be 92 pA ± 1 pA at 100 V reverse bias and 20 °C.

The explanation of the difference in the predicted β^- particle created currents and the experimental β^- particle created currents of the 0.06 mm^2 photodiode is still not known with absolute certainty. However, the experimentally measured β^- particle created currents were found to be greater at higher temperatures (see Fig. 2). In part, this may be explained by the average energy consumed in the generation of an electron-hole pair (the quantity commonly called the electron-hole pair creation energy) reducing with increasing temperature [25-26]. Assuming Si, GaAs, and 4H-SiC have a linear relationship between the electron-hole pair creation energy and the bandgap energy at 100 °C, the electron-hole pair creation energy of 4H-SiC at this temperature can be estimated to be 7.24 eV. Therefore, at 100 °C, the predicted β^- particle created current for the 0.06 mm^2 photodiode (active region thickness = 5.15 µm) would increase to 13.5 pA from 12.5 pA at 20 °C. However, the apparent β^- particle created currents in the detector showed a much more significant increase at reverse biases > 60 V at temperatures > 40 °C. As such, this effect may be due to the variation of the leakage component of the current which may have varied between measurement in dark condition and measurement when illuminated with the ^{63}Ni radioisotope β^- particle source. If the leakage component of the current was greater in the measurement with the device illuminated than when the device was measured in dark condition it would have produced an apparently (but not truly) greater β^- particle created current. However, a variation in leakage current of such size would be surprising. Use of a chopper wheel and lock-in amplifier apparatus to measure the response of the photodiode in both dark and illuminated condition within one experiment would

have eliminated any effects from this, but regrettably we do not possess such equipment at our laboratory at present.

3.3. ^{63}Ni β^- particle spectroscopy

The detector was connected to a custom-made low-noise charge-sensitive preamplifier with a wire-ended packaged 2N4416A silicon input JFET (capacitance = 2 pF) and installed in a TAS Micro MT climatic cabinet for temperature control as per the current-mode measurements. The preamplifier was of feedback resistorless design similar to Ref. [27]. An ORTEC 572A shaping amplifier and an ORTEC EASY-MCA 8k multi-channel analyser (MCA) were connected to the preamplifier's output.

The distance between the ^{63}Ni radioisotope β^- particle source and the photodiode's top surface was 4.5 mm ± 1.0 mm. The accumulation live time for each ^{63}Ni β^- particle spectrum was 720 s. The β^- particle spectra were accumulated at the temperatures from 100 °C to 20 °C with 20 °C decrements. Since the accumulated spectra at each temperatures were relatively similar, for clarity only the spectra accumulated at 100 °C and 20 °C are presented in Fig. 3. The shaping time of the shaping amplifier was set at 1 μs for the spectrum accumulated at 100 °C and at 2 μs for 20 °C. The results demonstrated that these detectors can be used as detectors for particle counting β^- (electron) spectroscopy at temperatures up to 100 °C.

Effects such as the change in electron-hole pair creation energy with temperature, and the change in preamplifier conversion factor with temperature will have been responsible in part for the change in apparent end point channel between temperatures. A degradation in the energy resolution of the spectrometer at higher temperatures (as was reported for the devices when used for photon counting X-ray spectroscopy [19]), will have blurred the end point channel more at higher temperatures than at lower temperatures. Furthermore, changing the shaping time of the shaping amplifier will have also effectively changed the width of the MCA channels in terms of eV per channel. The variation with temperature of the densities of the ^{63}Ni radioisotope β^- particle source, the N_2 atmosphere, and the detector will also have had some small effects (e.g. the lower density of the N_2 atmosphere at higher temperatures will have resulted in reduced energy losses in the N_2) but they are expected to have been less significant in effect than the changes in the other aspects outlined above.

In Section 5, the experimentally obtained ^{63}Ni β^- particle spectrum at 20 °C is compared with the spectrum predicted from the Monte Carlo modelling in Section 4.

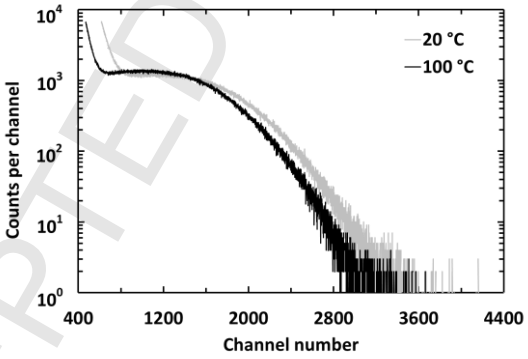

Fig. 3. ^{63}Ni β^- spectra obtained with the 0.06 mm^2 photodiode at 100 V reverse bias at 20 °C (grey line) and 100 °C (black line).

4. CASINO simulations

The trajectories of electrons (β^- particles) passing through materials can be simulated using the CASINO computer program [28-29]. Such simulations can be used to give an indication of how the structure of the photodiode (e.g. thickness of dead layers and active layers) affected the total energy deposited in the active layer of the device and hence what charge was detected. Electron energy losses in the photodiode's contact were negligible because it had an optical window. However, the β^- particles did lose energy as they travelled between the atom from which they were emitted and the photodiode. These energy losses occurred through self-absorption in the ^{63}Ni radioisotope β^- particle source [30], in the 1 μm thick protective inactive nickel overlayer of the source (density = 8.908 g/cm^3 at room temperature [31]), and in the dry N_2 atmosphere (density = 0.0012 g/cm^3 at room temperature [32]). Simulations were conducted to model these effects.

The aims of the simulations were to predict (a) the electron spectrum incident on the photodiode (i.e. taking into account energy losses from self-absorption, the inactive Ni overlayer, and the dry N_2 atmosphere), and (b) the electron spectrum detected by the photodiode to account for the fact that the remaining energy of the electrons may not have been fully absorbed by the relatively thin photodiode. The simulations tracked the path of each simulated electron through the various media and recorded the quantities and locations of the deposited energy along each track. The simulations were parallelised across 10 computers with Intel Core i7-6700 CPUs. Each computer had 32 GB of random access memory. As per Section 3.2, since there was doubt about the thickness of the detector's active region simulations were conducted to model three different active region thickness: (a) 5.15 μm, (b) 2.37 μm, and (c) 34.5 μm.

The simulations were conducted in three stages. Firstly, the electron (β^- particle) quantum efficiency of the photodiode in each case was computed. Secondly, the electron (β^- particle) spectrum expected to reach the detector was computed. Thirdly, the first and second stages were combined to predict the detected spectrum (excluding the noise processes known to broaden the energy resolution of photodiode radiation detectors i.e. Fano noise, electronic noise, and charge trapping noise [1]).

In the first stage, for electron energies from 1 keV to 66 keV, in 1 keV steps, 4000 electrons at each energy were simulated to be incident on the face of the photodiode. The quantum efficiency of the photodiode at each energy, defined as the ratio between the energy deposited in the active region and the energy incident on the photodiode, was computed. The results are presented in Fig. 4 for the active region thicknesses outlined above. The quantum efficiency in each case was found to be similar at energies < 20 keV. At these energies, the quantum efficiency in all three cases was > 90%. At energies > 20 keV and > 30 keV, the quantum efficiencies associated with the 2.37 μm and 5.15 μm active region thicknesses, respectively, were reduced.

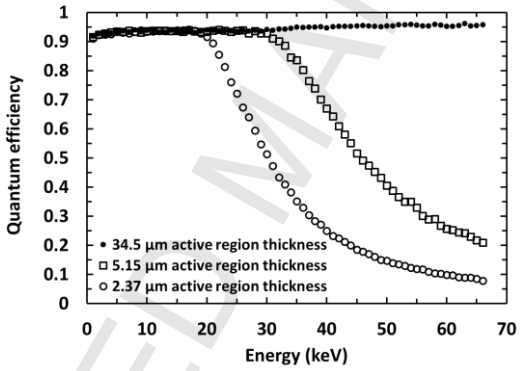

Fig. 4. Electron (β^- particle) quantum efficiency computed for the detector assuming active region thicknesses of 34.5 μm (filled circles), 5.15 μm (open squares), and 2.37 μm (open circles).

In the second stage, the spectrum of electron energies incident on the detector from the ^{63}Ni radioisotope β^- particle source was simulated. Electrons were simulated to be emitted from the ^{63}Ni at energies from 1 keV to 66 keV in 1 keV steps in the relative emission ratios for ^{63}Ni and taking account of self-absorption [24]. A total of 1.84×10^7 electrons were simulated to be emitted. Passage of the electrons through the 1 μm thick inactive Ni overlayer and the 4.5 mm thick N_2 atmosphere was simulated. For every electron which was not entirely absorbed in the Ni overlayer or the N_2 atmosphere, the energy remaining after the transmission was stored in the computer. The dataset was then binned into energy channels of 1 keV width to produce a histogram showing the distribution of remaining electron energies. This histogram is the spectrum of electron energies predicted to be incident on the detector. It is shown in Fig. 5 together with the ^{63}Ni emission spectrum taking into account the self-absorption of the source.

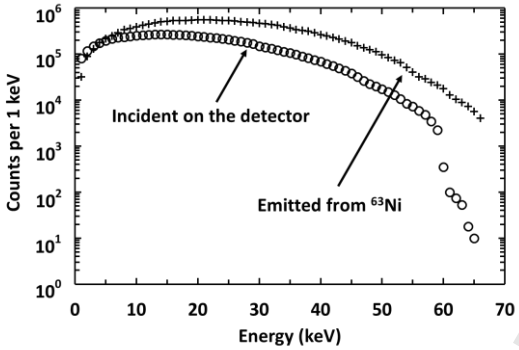

Fig. 5. Comparison between the β^- particle spectra emitted from the ^{63}Ni radioisotope β^- particle source including self-absorption but excluding attenuation in the 1 μm inactive overlayer (+ symbols) and incident on the top of the photodiode taking into account losses in the 1 μm inactive overlayer and the N_2 atmosphere (open circles).

In the third (and final) stage, the results of the first two stages were combined to produce the spectra predicted to be detected by the spectrometer for each simulated photodiode active layer thicknesses. The predicted spectra exclude effects such as pulse pile-up, noise processes, and detector edge effects. The spectra are shown in Fig. 6.

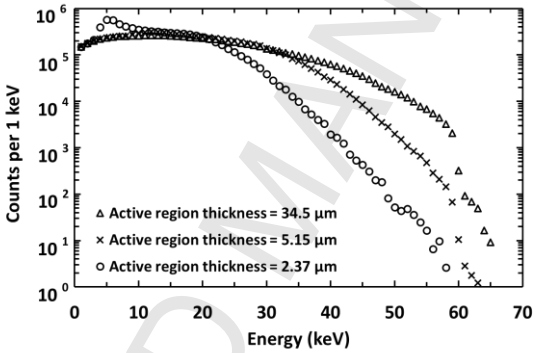

Fig. 6. Comparison of the β^- particle spectra predicted to be detected by the spectrometer in the case that the detectors active region thickness is 34.5 μm (open triangles), 5.15 μm (× symbols), and 2.37 μm (open circles). The spectra do not include effects such as pulse pile-up, noise processes, and detector edge effects.

For the simulations of the 34.5 μm and 5.15 μm active region thickness, the spectra had smooth shapes at detected energies up to 59 keV. However, the 2.37 μm active region thickness simulations predicted an increased number of counts around 5 keV. This is a consequence of the thinner active region detecting only a portion of the energy of electrons with greater total energy; that is to say that there is an increased likelihood that the β^- particles in this case deposit only ~ 5 keV in the detector before leaving the active region in this case. A further interesting feature of the spectra corresponding to the 34.5 μm and 5.15 μm cases is the rapid decrease in detected counts at energies > 59 keV. Whilst the emission spectrum of ^{63}Ni does rapidly reduce at energies close to its endpoint energy, a further effect is at work in the spectra shown in Fig. 6. Here, the natural rapid drop is enhanced by the low and compounding probabilities of electrons retaining such large amounts of energy after their passage through the source's inactive overlayer and the 4.5 mm thick N_2 layer, and then depositing such large amounts of energy in the detector.

5. Comparison of simulation and experimental results

The simulated detected β^- spectrum was then compared with the experimentally accumulated spectrum at 20 °C. The heights of the simulated spectra have been normalised to the experimental spectrum by the same factor to take account of the accumulation time of the experimental spectrum and the ^{63}Ni radioisotope β^- particle source's activity. The comparison is presented in Fig. 7.

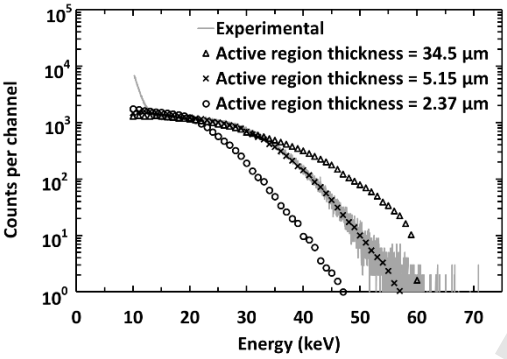

Fig. 7. Comparison between the experimentally detected ^{63}Ni β^- particle spectrum at 20 °C (grey solid line), and the simulated spectra assuming active region thicknesses of: 34.5 µm (open triangles), 5.15 µm (× symbols), and 2.37 µm (open circles).

Comparing the shapes of the β^- spectra simulated using the CASINO simulations and the spectrum experimentally obtained at a temperature of 20 °C, it can be seen that the simulation using an active region thickness of 5.15 µm produces a good agreement with experimental β^- particle spectrum. In contrast, the simulations using active region thicknesses of 2.37 µm and 34.5 µm do not match the experimental spectrum. As such, this is an indication that the thickness of the active region of the detector was 5.15 µm, which is the thickness of the epilayer as stated by manufacturer. The few detected counts seen in the spectrum above 57 keV may be due to the statistical effects of pulse pile-up and other noise contributions.

6. Conclusions

A commercial 4H-SiC p-n photodiode with an active area of 0.06 mm^2 was investigated as current mode and pulse mode detector of β^- particles over the temperature range 100 °C to 20 °C.

The leakage currents as functions of applied reverse bias for the device was studied at different temperatures, and the results showed the leakage currents of the device decreased with decreasing temperature. At the highest investigated temperature (100 °C), the leakage current of this device was found to be < 45 pA (corresponding to leakage current density of 75 nA/cm^2) at 100 V reverse bias. The performance of the device as temperature tolerant electron detector was investigated by measuring the β^- generated current whilst the device was illuminated by a ^{63}Ni radioisotope β^- particle source. At the highest investigated reverse bias (100 V), the apparent β^- particle generated current in the 0.06 mm^2 photodiode was found to be 92 pA ± 1 pA at a temperature of 20 °C. However, doubt exists whether the extra current measured with the photodiode illuminated can be entirely attributed to the β^- particles, or if there was some increase in the leakage current component as well.

The photodiode was connected to a custom-made low-noise charge-sensitive preamplifier and found to function as electron spectrometer under the illumination of a ^{63}Ni radioisotope β^- particle source across the temperature range of 100 °C to 20 °C. The CASINO computer program was used to calculate the quantum efficiency of the photodiode assuming three different active region thicknesses (5.15 µm, 2.37 µm, and 34.5 µm). CASINO was also used to simulate the β^- particle spectra incident upon, and detected by, the photodiode. Agreement was found between the experimentally measured and simulated ^{63}Ni β^- particle spectra when a detector active region thickness of 5.15 µm was simulated. This suggests that the entire 5.15 µm thick epilayer is sensitive to β^- particles, but that β^- particles absorbed in the substrate are lost.

The results demonstrate that this type of low-cost COTS SiC photodiode can be coupled to a low-noise charge-sensitive preamplifier and standard signal processing electronics (a shaping amplifier and an MCA), to produce spectrometer which can detect electrons of energy up to 57 keV. This lays the foundations for university groups and other cost-sensitive organisations to use such devices as detectors for CubeSat space plasma physics missions, or for commercial organisations to use such detectors for industrial electron spectroscopy.

Acknowledgements

This work was in part supported by the Science and Technologies Facilities Council, United Kingdom, through grants ST/M004635/1 and ST/P001815/1 (University of Sussex, A.M.B., PI). M.D.C. Whitaker acknowledges

funding received from the University of Sussex in the form of a PhD scholarship. A.M.B. acknowledges funding from the Leverhulme Trust in the form of a 2016 Philip Leverhulme Prize.

References

[1] A. Owens, Compound Semiconductor Radiation Detectors, CRC Press, Boca Raton, 2012.
[2] T. Seyller, Electronic properties of SiC surfaces and interfaces: some fundamental and technological aspects, Applied Physics A, 85 (2006) 371-385.
[3] G. Bertuccio, and R. Casiraghi, Study of Silicon Carbide for X-Ray Detection and Spectroscopy, IEEE Transactions on Nuclear Science, 50 (2003) 175-185.
[4] F. Nava, et al., Radiation tolerance of epitaxial silicon carbide detectors for electrons, protons and gamma-rays, Nuclear Instruments and Methods in Physics Research, Section A, 505 (2003) 645-655.
[5] G. Bertuccio, et al., Silicon carbide detector for laser-generated plasma radiation, Applied Surface Science, 272 (2013), 128-131.
[6] M. Rogalla, et al., Particle detectors based on semi-insulating silicon carbide, Nuclear Physics B - Proceedings Supplements, 78 (1999) 516-520.
[7] F. Nava, et al., Minimum ionizing and alpha particles detectors based on epitaxial semiconductor silicon carbide, IEEE Transactions on Nuclear Science, 51 (2004) 238-244.
[8] M. Bruzzi, et al., Characterisation of epitaxial SiC Schottky barriers as particle detectors, Diamond and Related Materials, 12 (2003) 1205-1208.
[9] B. Zat'ko, et al., High resolution alpha particle detectors based on 4H-SiC epitaxial layer, Journal of Instrumentation, 10 (2015) C04009.
[10] F.H. Ruddy, et al., High-resolution alpha-particle spectrometry using 4H silicon carbide semiconductor detectors, IEEE Transactions on Nuclear Science, 53 (2006) 1713-1718.
[11] Y.M. Abubakar, et al., Stability of silicon carbide particle detector performance at elevated temperatures, IEEE Transactions on Nuclear Science, 62 (2015) 2360-2366.
[12] G. Bertuccio, et al., Silicon carbide for high resolution X-ray detectors operating up to 100 °C, Nuclear Instruments and Methods in Physics Research, Section A, 522 (2004) 413-419.
[13] G. Bertuccio, et al., Advances in silicon carbide X-ray detectors, Nuclear Instruments and Methods in Physics Research, Section A, 652 (2011) 193-196.
[14] L.Torrisi, et al., Laser-plasma X-ray detection by using fast 4H-SiC interdigit and ion collector detectors, Journal of Instrumentation, 10 (2015) P07009.
[15] A. Cannavò, et al., Characterization of X-ray emission from laser generated plasma, EPJ Web of Conferences, 167 (2018) 03004.
[16] L.Torrisi, and A. Cannavò, SiC detector damage and characterization for high intensity laser-plasma diagnostics, Journal of Instrumentation, 11 (2016) P05009.
[17] A. Sciuto, et al., Effects induced by high and low intensity laser plasma on SiC Schottky detectors, EPJ Web of Conferences, 167 (2018) 03005.
[18] S. Zhao, et al., Soft X-ray detection and photon counting spectroscopy with commercial 4H-SiC Schottky photodiodes, Nuclear Instruments and Methods in Physics Research, Section A, 830 (2016) 1-5.
[19] S. Zhao, et al., Temperature dependence of commercial 4H-SiC UV Schottky photodiodes for X-ray detection and spectroscopy, Nuclear Instruments and Methods in Physics Research, Section A, 859 (2017) 76-82.
[20] S. Zhao, et al., X-ray spectrometer with a low-cost SiC photodiode, Nuclear Instruments and Methods in Physics Research, Section A, 887 (2018) 138-143.
[21] Anon, Broadband SiC based UV photodiode A=0.06 mm^2, SG01S–18, Rev.6.0, SGlux SolGel Technologies GmbH, Berlin, Germany. N.D.
[22] D. Prasai, et al., Highly reliable silicon carbide photodiodes for visible-blind ultraviolet detector applications, Journal of Materials Research, 28 (2013) 33-37.
[23] T.R. Alam, and M.A. Pierson, Principles of Betavoltaic Battery Design, Journal of Energy and Power Sources, 3 (2016) 11-41.
[24] Y. Liu, et al., Influences of planar source thickness on betavoltaics with different semiconductors, Journal of Radioanalytical and Nuclear Chemistry, 304 (2015) 517-525.
[25] R.C. Alig, and S. Bloom, Electron-hole-pair creation energies in semiconductors, Physical Review Letters, 35 (1975) 1522-1525.
[26] M.E. Levinshtein, et al., Properties of Advanced Semiconductor Materials: GaN, AIN, InN, BN, SiC, SiGe, John Wiley & Sons, 2001.
[27] G. Bertuccio, et al., A novel charge sensitive preamplifier without the feedback resistor, Nuclear Instruments and Methods in Physics Research, Section A, 326 (1993) 71-76.
[28] P. Hovington, et al., CASINO: A new Monte Carlo code in C language for electron beam interaction - Part I: Description of the program, Scanning, 19 (1997) 1-14.

[29] D. Drouin, et al., CASINO: A new Monte Carlo code in C language for electron beam interactions - Part II: Tabulated values of the mott cross section, Scanning, 19 (1997) 20-28.
[30] G.H.E. Sims, and D.G. Juhnke, The beta self-absorption of Ni^{63} as metallic nickel, The International Journal Of Applied Radiation And Isotopes, 18 (1967) 727-728.
[31] N.N. Greenwood, and A. Earnshaw, Chemistry of the Elements, Butterworth-Heinemann, 1997.
[32] B.A. Younglove, and N.A. Olien, Tables of Industrial Gas Container Contents and Density for Oxygen, Argon, Nitrogen, Helium, and Hydrogen, National Institute of Standards and Technology, Gaithersbury, Maryland, USA, 1985.

Figure captions

Fig. 1. Leakage currents as functions of applied reverse bias for the 0.06 mm^2 photodiode in the range of temperature from 100 °C to 20 °C.

Fig. 2. Measured apparent β^- particle created currents as functions of reverse bias for the 0.06 mm^2 photodiode in the range of temperature from 100 °C to 20 °C.

Fig. 3. ^{63}Ni β^- spectra obtained with the 0.06 mm^2 photodiode at 100 V reverse bias at 20 °C (grey line) and 100 °C (black line).

Fig. 4. Electron (β^- particle) quantum efficiency computed for the detector assuming active region thicknesses of 34.5 μm (filled circles), 5.15 μm (open squares), and 2.37 μm (open circles).

Fig. 5. Comparison between the β^- particle spectra emitted from the ^{63}Ni radioisotope β^- particle source including self-absorption but excluding attenuation in the 1 μm inactive overlayer (+ symbols) and incident on the top of the photodiode taking into account losses in the 1 μm inactive overlayer and the N_2 atmosphere (open circles).

Fig. 6. Comparison of the β^- particle spectra predicted to be detected by the spectrometer in the case that the detectors active region thickness is 34.5 μm (open triangles), 5.15 μm (× symbols), and 2.37 μm (open circles). The spectra do not include effects such as pulse pile-up, noise processes, and detector edge effects.

Fig. 7. Comparison between the experimentally detected ^{63}Ni β^- particle spectrum at 20 °C (grey solid line), and the simulated spectra assuming active region thicknesses of: 34.5 μm (open triangles), 5.15 μm (× symbols), and 2.37 μm (open circles).